Open Ceramics 11 (2022) 100289

Contents lists available at ScienceDirect

Open Ceramics

journal homepage: www.sciencedirect.com/journal/open-ceramics

# Densification behavior of monolithic SiC fabricated by pressureless liquid phase sintering method

Jun-Yeab Lee *, Tatsuya Hinoki

*Kyoto University, Japan*

ARTICLE INFO

*Keywords:*
Pressureless liquid phase sintering
Silicon carbide
Microstructure analysis
Isotropic shrinkage
Mechanical properties

ABSTRACT

As a preliminary investigation of process development for SiC fiber-reinforced SiC matrix composites ($SiC_f$/SiC composites) via a pressureless liquid phase sintering (PLPS) method, the manufacturing process parameters of monolithic SiC fabricated with/without very low pressure during the sintering under high temperature (1850 and 1900 °C) were optimized. Two kinds of sintering additive system (only $Al_2O_3$ and $Al_2O_3$–$Y_2O_3$ mixtures) can be achieved full densification corresponding to 99% of the theoretical density without high pressure during the sintering. Monolithic SiCs of both sintering additive systems applied with prepressure of 20 or 40 MPa possessed the flexural strength and porosity comparable to those of conventional liquid-phase sintered SiC with high pressure during the sintering. The low pressure (0.63 MPa) during sintering reduced the densification in particular for the materials sintered with just $Al_2O_3$. The additions of BN particles led to a gradual decrease in mechanical strength with an increase in porosity.

## 1. Introduction

Silicon carbide (SiC) based ceramic matrix composites (CMCs) are the candidate materials for hot sections components of aviation engines, nuclear fission reactors (light water reactor and Generation Ⅳ nuclear power plants), and nuclear fusion applications due to their superior properties such as neutron irradiation resistance, corrosion resistance, chemical stability, oxidation resistance, and low radioactivity [1–5]. In recent years, aircraft engine's efficiency has been continuously demanded, along with global environmental problems. In contrast to current Ni-based superalloys, lighter weight CMCs components such as combustor liner, shrouds, turbine blades, and vanes allow operating at higher temperatures and higher pressure ratios with reduced cooling air. In shorts, the increased engine efficiency would result in lower $CO_2$ emissions and effective cost savings due to less fuel consumption in the aircraft's operating environment [6,7]. SiC-based CMCs reinforced with various types of fibers and fabrics have been provided and studied with various manufacturing methods such as chemical vapor infiltration (CVI), polymer impregnation and pyrolysis (PIP), and slurry melt infiltration (SMI). However, since the SiC-based CMCs fabricated by the CVI process has a residual porosity of about 20%, the increase in manufacturing cost due to the long processing time has been a problem in order to overcome such material defects. The PIP process also has a disadvantage in that crystals constituting the microstructure are formed in amorphous (α- and β-SiC) form along with the long-time process by a plurality of cycles for high density. In the case of SMI process, since residual silicon regions exist within the material, high temperature mechanical properties are determined by them. Hot-pressing via a liquid phase sintering (LPS) at the eutectic point of sintering additives has been recently used to produce the dense SiC-based CMCs [8–12]. SiC-based CMCs fabricated by the LPS method through hot-pressing exhibits a high level of density and strength but have disadvantages such as difficulty in manufacturing complex shapes due to the use of high pressure during the sintering. The material degradation is caused by the oxidation of interphase between the matrix and the fiber at high temperature [13,14,15]. On the other hand, boron nitride (BN) particle dispersion $SiC_f$/SiC composites fabricated with prepreg technique can provide excellent oxidation resistance and mechanical properties even at high temperature [16].

To overcome the manufacturing difficulty of LPS, the pressureless liquid phase sintering (PLPS) method that doesn't use pressure when hot-pressing at high temperature is expected to be newly applied [17]. H. Liang et al. [18] investigated the effect of the addition of $TiO_2$ particles as a Ti source to the α-SiC matrix using the PLPS process and reported that the sample was densified to nearly theoretical density by PLPS process using the $Al_2O_3$, $Y_2O_3$, and $TiO_2$ additives. The SiC–$TiO_2$

* Corresponding author.
*E-mail address:* lee.junyeab.3s@kyoto-u.ac.jp (J.-Y. Lee).

https://doi.org/10.1016/j.oceram.2022.100289
Received 26 April 2022; Received in revised form 21 June 2022; Accepted 26 June 2022
Available online 30 June 2022

**Table 1**
The detailed material compositions, prepressing, and sintering conditions of monolithic SiC fabricated in this study.

| Material ID | | Sintering additive | | BN powder | Pre-pressing | | Sintering | | |
|---|---|---|---|---|---|---|---|---|---|
| | | $Al_2O_3$ (wt. %) | $Y_2O_3$ (wt. %) | (vol%) | Pressure (MPa) | Time (min) | Temperature (°C) | Pressure (MPa) | Time (min) |
| LPS-SiC | AY020 | 6 | 4 | – | – | – | 1850 | 20 | 60 |
| | A020 | 12 | – | – | – | – | 1900 | 20 | 60 |
| PLPS-SiC with low-pressure | AY201 | 6 | 4 | – | 20 | 30 | 1850 | 0.63 | 60 |
| | AY401 | 6 | 4 | – | 40 | 30 | 1850 | 0.63 | 60 |
| | A201 | 12 | – | – | 20 | 30 | 1900 | 0.63 | 60 |
| | A401 | 12 | – | – | 40 | 30 | 1900 | 0.63 | 60 |
| | 1BNAY401 | 6 | 4 | 1 | 40 | 30 | 1850 | 0.63 | 60 |
| | 10BNAY401 | 6 | 4 | 10 | 40 | 30 | 1850 | 0.63 | 60 |
| | 20BNAY401 | 6 | 4 | 20 | 40 | 30 | 1850 | 0.63 | 60 |
| PLPS-SiC with no-pressure | AY00 | 6 | 4 | – | – | – | 1850 | – | 60 |
| | AY200 | 6 | 4 | – | 20 | 30 | 1850 | – | 60 |
| | AY400 | 6 | 4 | – | 40 | 30 | 1850 | – | 60 |
| | 0AY400 | – | – | – | 40 | 30 | 1850 | – | 60 |
| | 1AY400 | 0.6 | 0.4 | – | 40 | 30 | 1850 | – | 60 |
| | 5AY400 | 3 | 2 | – | 40 | 30 | 1850 | – | 60 |
| | A00 | 12 | – | – | – | – | 1900 | – | 60 |
| | A200 | 12 | – | – | 20 | 30 | 1900 | – | 60 |
| | A400 | 12 | – | – | 40 | 30 | 1900 | – | 60 |
| | 1BNAY400 | 6 | 4 | 1 | 40 | 30 | 1850 | – | 60 |
| | 10BNAY400 | 6 | 4 | 10 | 40 | 30 | 1850 | – | 60 |
| | 20BNAY400 | 6 | 4 | 20 | 40 | 30 | 1850 | – | 60 |

samples exhibited increased fracture toughness due to the elongated growth of SiC particles by the in-situ formed TiC particles and increasing the residual thermal stress due to the mismatched thermal expansion coefficients of SiC and TiC particles. K. J. Kim et al. [19] also studied PLPS-SiC ceramics using the $Al_2O_3$–$Y_2O_3$–AlN additives and reported that the SiC specimen with a relative density of 97% was composed mainly of 6H- and 4H–SiC grains surrounded by amorphous Al–Y–Si–O–C–N thin films. The SiC $Al_2O_3$–AlN–$Y_2O_3$ samples exhibited electrical resistivity as high as $1.2 \times 10^{13}$ Ω cm at room temperature. The above-mentioned studies used a high level of prepressure along with the cold isostatic pressing (CIP) process before sintering and were studied to improve the fracture toughness and to investigate the electrical resistivity of the monolithic SiC ceramics only. However, the effects of various manufacturing parameters on matrix consolidation via the PLPS process to apply $SiC_f$/SiC composites fabrication have not been understood. The maximum processing temperature is limited by high temperature stability of SiC fibers. The influence of prepressure magnitude and its densification behavior in PLPS-SiC remain unclear. The effect of BN addition for the SiC composites matrix on sintering by PLPS has not been understood.

This study presents a preliminary investigation of monolithic SiC manufactured by the PLPS method with the various process parameters, including kinds and amounts of sintering additives, pre-and sintering pressure, and amounts of BN addition for the matrix consolidation of $SiC_f$/SiC-matrix composites. The microstructural analyses, densification behavior, and mechanical properties of the PLPS-SiC were investigated to uncover the relationship between the process parameters and matrix consolidation. All of the experimental data were compared with the well-known 'rule of mixtures (ROM) theory.

## 2. Experimental procedure

Three types of monolithic SiC were fabricated under high temperatures via a LPS process: pressure-assisted monolithic SiC using the 20 MPa of pressure during the sintering, and low-pressed or no-pressed during sintering monolithic SiC with uniaxially cold-pressing before sintering. These materials are referred to as LPS-SiC (pressure-assisted monolithic SiC using the pressure of 20 MPa during the sintering), PLPS-SiC with low-pressure (low-pressed monolithic SiC using the pressure of 0.63 MPa during the sintering), and PLPS-SiC without pressure (no-pressed monolithic SiC), respectively. Low pressure of 0.63 MPa was used to provide the constrained sintering environment by loading the z-direction of the sample for comparison with the materials in an unconstrained environment. A very high purity SiC nano-powder with the hexagonal α-type crystal (GC#40000, Fujimi Incorporated, Japan) was employed as a raw material for the PLPS-SiC fabricated in this study. Two kinds of sintering additives were prepared for comparison. As for $Al_2O_3$–$Y_2O_3$ (AY) material, $Al_2O_3$ (mean particle size = 0.3 μm, Kojundo Chemical Laboratory Co. Ltd, Japan) and $Y_2O_3$ (mean particle size = 0.4 μm, Kojundo Chemical Laboratory Co. Ltd, Japan) were used as the sintering additives, and as for $Al_2O_3$ (A) materials, 12 wt% of only $Al_2O_3$ was used as the sintering additive. The $Al_2O_3$:$Y_2O_3$ weight ratio in the $Al_2O_3$–$Y_2O_3$ additives was 3:2. In addition to evaluate the effect of weight fraction of sintering additives on densification behavior, different weight fractions of 0, 1, 5, and 10 wt% were used for comparison in the $Al_2O_3$–$Y_2O_3$ additive materials. As the reference of matrix in the BN particle dispersion $SiC_f$/SiC composites, BN particles of different volume fractions (0, 1, 10, and 20 vol%) were also used in the fabrication of PLPS-SiCs. The mixture slurries were prepared and dried in air and uniaxially prepressed with 0, 20, and 40 MPa into graphite-die at room temperature. All of AY materials were sintered at 1850 °C for 1 h in Ar atmosphere, and all of A materials were sintered at 1900 °C for 1 h in Ar. The detailed compositions, processing, and sintering conditions are summarized in Table 1.

Each process's packing density and linear shrinkage were calculated by geometric dimensions and weight of powder compact. The density and porosity of fabricated specimens were measured by a gas pycnometer (Accupyc II 1340, Micromeritics, U.S.A.) using helium gas. The theoretical densities of each material were calculated by the ROM. Sintered samples were cut and polished, and were then etched using the plasma-cleaner (PC-2000, South Bay Technology, U.S.A) by $CF_4$–$O_2$ mixture gas for microstructure observation. The mechanical strength of all specimens was obtained by a 4-point bending test (Instron 5581) based on ASTM C 1161. The 4-point bending test was performed using $2 \times 1.5 \times 25$ $mm^3$ specimens at constant displacement rate of 0.2 mm/min, support span length of 20 mm, and inner span length of 10 mm. The fracture and etched surfaces were observed by field-emission scanning electron microscopy (FE-SEM, Ultra 55, ZEISS, Germany).

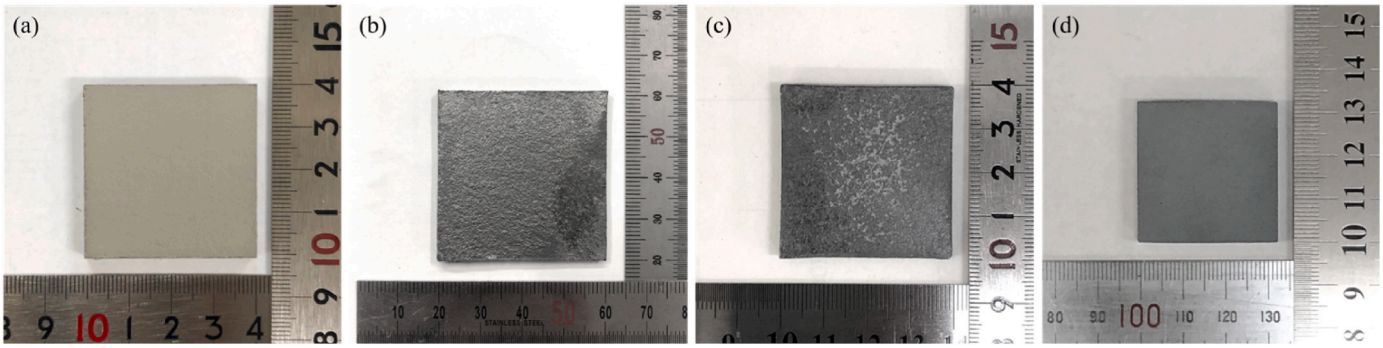


**Fig. 1.** Top view of a prepressed powder compact and three types of monolithic SiC: (a) prepressed powder compact, (b) LPS-SiC, (c) PLPS-SiC with low-pressure, and (d) PLPS-SiC without pressure.

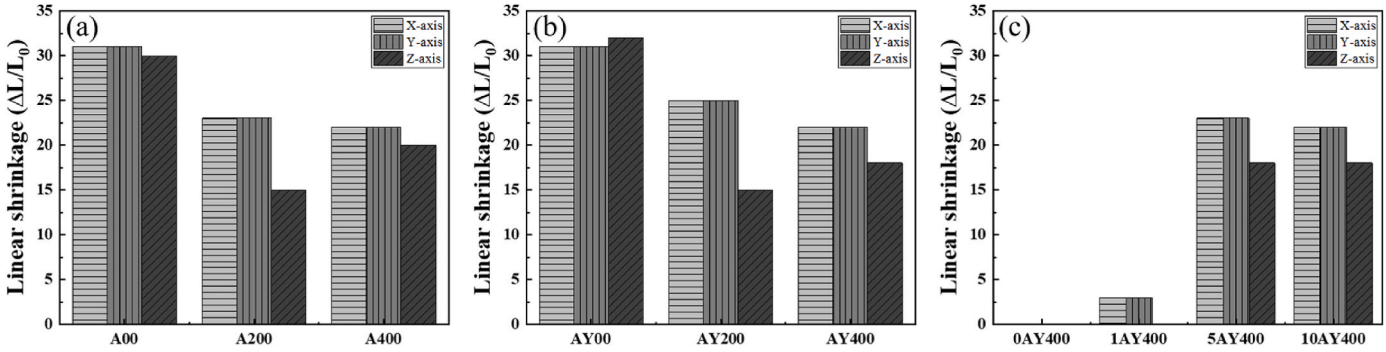


**Fig. 2.** Linear shrinkage from prepressing PLPS-SiC without pressure with different kinds and amounts of sintering additives. (a) only $Al_2O_3$, (b) $Al_2O_3$–$Y_2O_3$ mixtures, and (c) different amounts of $Al_2O_3$–$Y_2O_3$ mixtures.

## 3. Results

### 3.1. Liner shrinkage and packing density

Processing parameters of LPS-SiC with high pressure during the sintering were firstly optimized in the previous studies. Low porosities with dense microstructure and high mechanical strength were achieved via the pressure-assisted LPS process using both sintering additives ($Al_2O_3$–$Y_2O_3$ and only $Al_2O_3$) [20–23]. The densification behavior of LPS-SiC can be improved by increasing the sintering temperature and/or applied sintering pressure. However, it is upper limited to the sintering temperature of 1850 °C and applied sintering pressure of 20 MPa for $Al_2O_3$–$Y_2O_3$ additives, and 1900 °C and 20 MPa for only $Al_2O_3$ additive in order to minimize fiber damage and obtain excellent densification when manufacturing $SiC_f$/SiC composites [11,23,24]. Fig. 1 shows the geometry and appearance of a prepressed powder compact and three types of as-fabricated monolithic SiC by LPS process. All of PLPS-SiC without pressure shrunk to all directions (Fig. 1(d)), since no external constrained force into the z-axis was used for this type of material. When the temperature reaches the eutectic point, the sintering additives dispersed in the green compact are melted, and the SiC particles are attracted to each other due to the capillary force exerted by the liquid on SiC particles [25]. All of LPS-SiC and PLPS-SiC with low-pressure shrunk to only the z-axis due to the external constrained force of 20 MPa and 0.63 MPa during the sintering, respectively and kept geometry of x- and y-axes from prepressed powder compact.

Linear shrinkage in all directions after prepressing and sintering were examined using the geometric information of the prepressed powder compact and as-sintered specimens. The similar level of linear shrinkage in the z-axis after prepressing was confirmed regardless of the process parameters such as the kinds and amount of the sintering additives, and BN particle additions. After prepressing, the linear

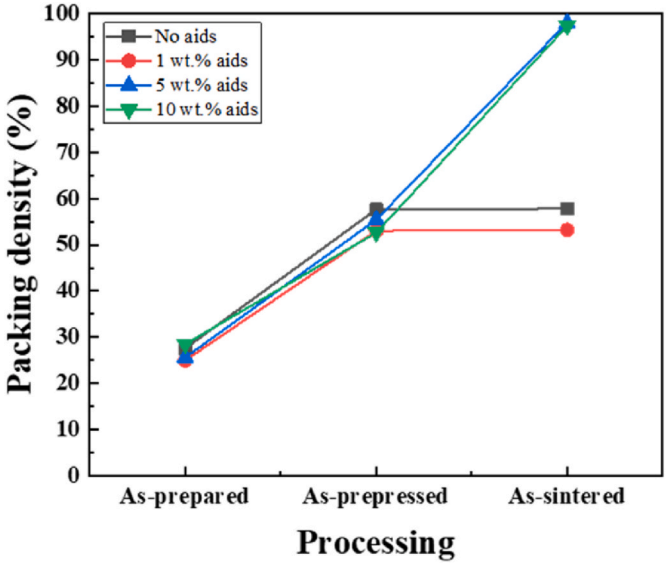


**Fig. 3.** Packing density of PLPS-SiC with different amounts of sintering additives ($Al_2O_3$–$Y_2O_3$ mixtures).

shrinkages of the powder compact applied prepressure with 20 MPa and 40 MPa were approximately 40% and 50%, respectively. Fig. 2 shows the linear shrinkage in all directions of PLPS-SiC without pressure after sintering. PLPS-SiC without prepressure and sintering pressure (A00 and AY00) showed isotropic shrinkage behavior (Fig. 2(a) and (b)). The prepressure of 20 and 40 MPa applied to the powder compacts prevented the isotropic shrinkage in the z-axis, but the shrinkage in the x- and y-axes were the same as shown in Fig. 2(a) and (b). Fig. 2(c) shows

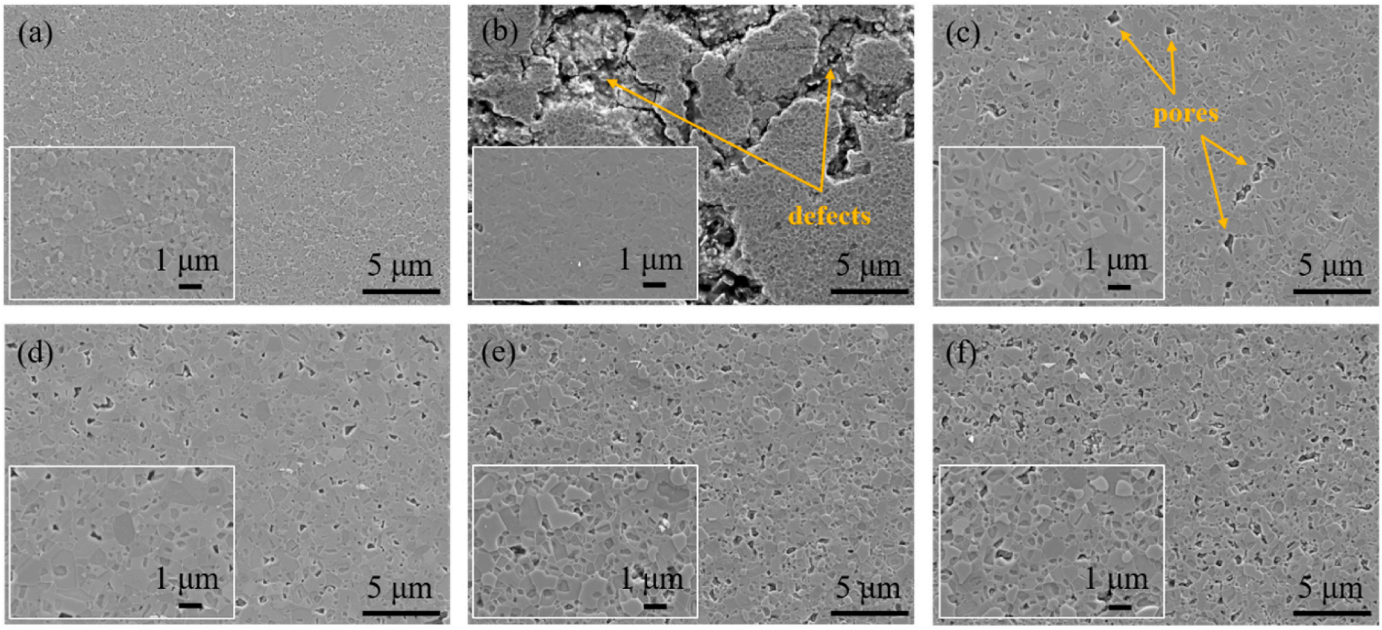


**Fig. 4.** Cross-sectional FE-SEM images of the monolithic SiC fabricated by different process parameters using only $Al_2O_3$ additive. (a) prepressure: 0 MPa and sintering pressure: 20 MPa, (b) prepressure: 0 MPa and sintering pressure: 0 MPa, (c) prepressure: 20 MPa and sintering pressure: 0 MPa, (d) prepressure: 40 MPa and sintering pressure: 0 MPa, (e) prepressure: 20 MPa and sintering pressure: 0.63 MPa, (f) prepressure: 40 MPa and sintering pressure: 0.63 MPa.

the linear shrinkage of PLPS-SiC with different amounts of sintering additives ($Al_2O_3$–$Y_2O_3$ mixtures of 0, 1, 5, and 10 wt%). The pressure conditions were applied in the same manner as the prepressure of 40 MPa and no sintering pressure (0 MPa). It was possible to confirm a marked difference in the shrinkage according to the weight fraction of the sintering additives. In 0AY400 and 1AY400 materials, 0 wt% and 1 wt% of sintering additives were not enough for shrinkage to obtain a high-density material, and 5AY400 and 10AY400 materials exhibited similar level of shrinkage even though the sintering additives had different weight fractions (Fig. 2(c)). Fig. 3 shows the packing density in each process of PLPS-SiC with different amounts of sintering additives.

As supporting the results in Fig. 2(c), PLPS-SiCs with $Al_2O_3$–$Y_2O_3$ mixtures of 5 and 10 wt% achieved full-densification by the sufficient amounts of sintering additives during the sintering. On the other hand, there are no or insufficient rearrangement and solution-reprecipitation stages of the LPS process to achieve the final densification by liquid phase formation in 0 and 1 wt% aids PLPS-SiCs. The packing densities of as-prepressed and as-sintered (bulk density) were almost the same even after sintering at high temperature in these cases.

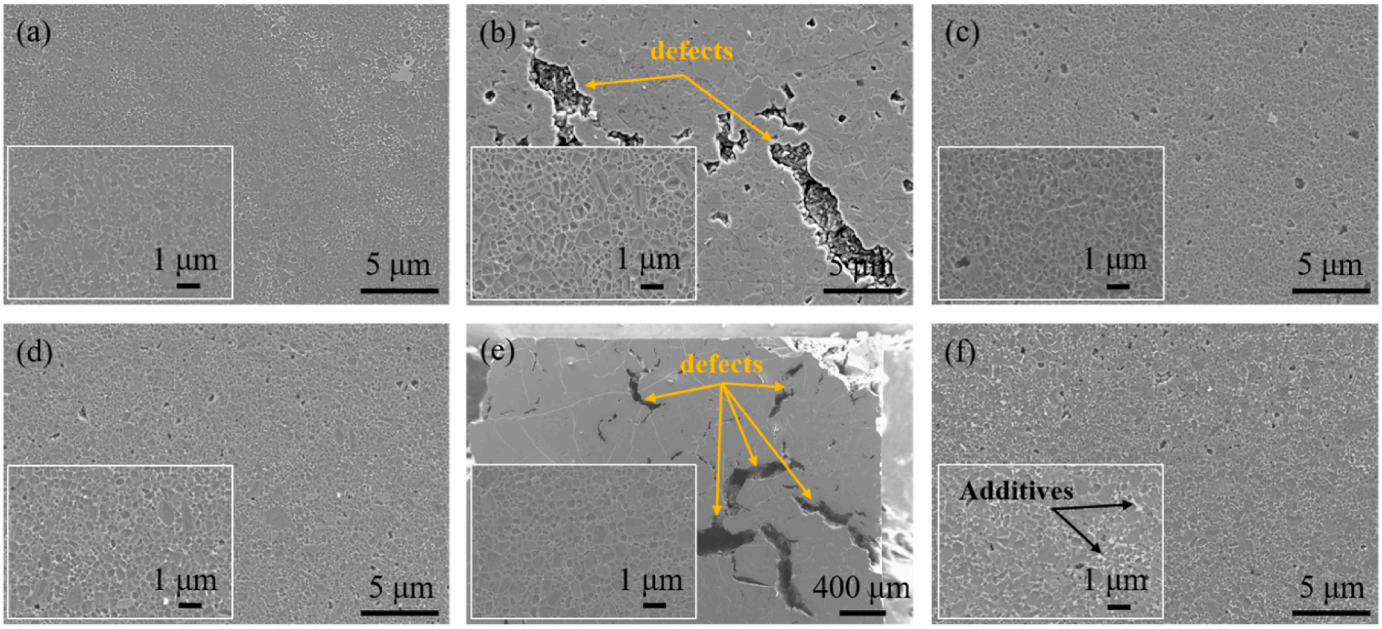


**Fig. 5.** Cross-sectional FE-SEM images of the monolithic SiC fabricated by different process parameters using $Al_2O_3$–$Y_2O_3$ additives. (a) prepressure: 0 MPa and sintering pressure: 20 MPa, (b) prepressure: 0 MPa and sintering pressure: 0 MPa, (c) prepressure: 20 MPa and sintering pressure: 0 MPa, (d) prepressure: 40 MPa and sintering pressure: 0 MPa, (e) prepressure: 20 MPa and sintering pressure: 0.63 MPa, (f) prepressure: 40 MPa and sintering pressure: 0.63 MPa.

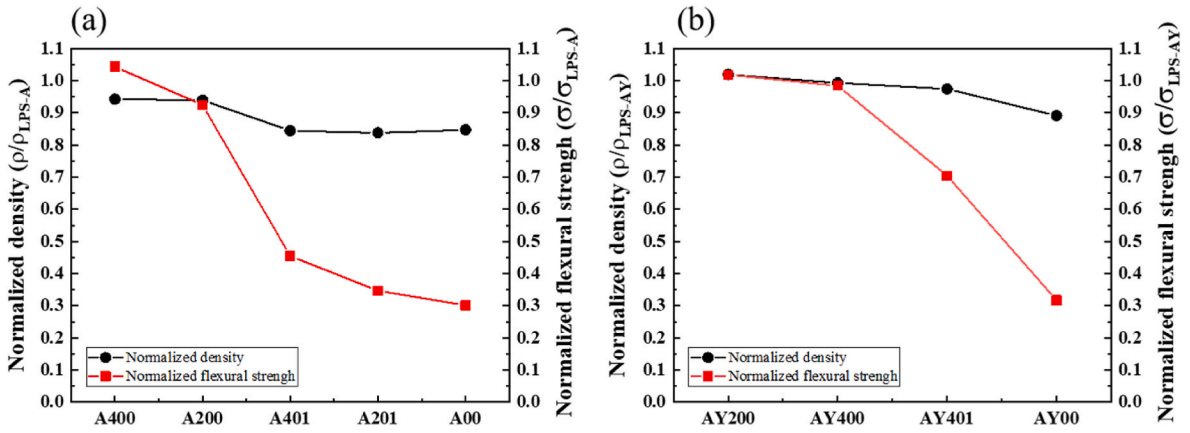


**Fig. 6.** Normalized relative density and flexural strength of PLPS-SiCs fabricated using (a) only $Al_2O_3$ additive, and (b) $Al_2O_3$–$Y_2O_3$ additives.

### 3.2. Microstructural and XRD analysis

Fig. 4 shows the cross-sectional microstructures images observed by FE-SEM of polished then etched monolithic SiC fabricated by different process parameters using only 12 wt% $Al_2O_3$ as the sintering additive. For LPS-SiC, the densest microstructure was observed, and it was difficult to confirm pores even at high magnification since the pressure of 20 MPa was assisted during the sintering (Fig. 4(a)). The cross-sectional image of PLPS-SiC without prepressure and sintering pressure was also observed as shown in Fig. 4(b). No dense microstructure was confirmed in PLPS-SiC without prepressure and sintering pressure, relatively large defects were observed. PLPS-SiCs with pressure and without sintering pressure show the dense microstructures compared with PLPS-SiC without prepressure and sintering pressure, only pores less than 1 μm can be observed, as shown in Fig. 4(c) and (d). For PLPS-SiCs with low-pressure, relatively large amounts of pores were observed compared with PLPS-SiCs without pressure, and also found that the measured porosities are higher than that of PLPS-SiCs without pressure. It is difficult to achieve full densification by isotropic shrinkage for the powder compacts constrained in the x- and y-axes due to the use of low pressure, and as a result, a relatively large amount of pores as shown in Fig. 4(e) and (f) were confirmed in the microstructure of PLPS-SiCs.

The cross-sectional FE-SEM images of monolithic SiC fabricated by different processing parameters using $Al_2O_3$–$Y_2O_3$ as the sintering additives are shown in Fig. 5. In this additive system, except for one processing parameter (Fig. 5(e)), it was possible to identify dense microstructures than monolithic SiC fabricated using only $Al_2O_3$ as the sintering additive. In the case of $Al_2O_3$–$Y_2O_3$ additives, a relatively large amount of extra sintering additives (bright phase) was observed in the microstructure between the liquid-phase sintered SiC grains, which is considered to affect the grain size of sintered SiC. For PLPS-SiC using only 12 wt% $Al_2O_3$ as the sintering additives, only the materials that did not use sintering pressure had the dense microstructure comparable to that of general pressure-assisted LPS-SiC as confirmed in Fig. 4(c) and (d), but it was different results when $Al_2O_3$–$Y_2O_3$ mixtures were used as the sintering additives. For PLPS-SiC using $Al_2O_3$–$Y_2O_3$ mixtures as the sintering additives, the material with the dense microstructure could be obtained, even in a constrained sintering environment with a pressure of 0.63 MPa, as shown in Fig. 5(f). In Fig. 5(e), the defects with a size of several hundred micrometers can be identified. Although materials were fabricated several times under the same conditions (prepressure: 20 MPa, sintering pressure: 0.63 MPa), all materials had defects, as shown in Fig. 5(e). When the amount of sintering additive was reduced from 10 wt% to 5 wt%, it was confirmed that these defects were remarkably reduced. The powder compact containing 10 wt% of $Al_2O_3$–$Y_2O_3$ additives applied with a prepressure of 20 MPa was sintered unstable in a constrained sintering environment with 0.63 MPa, which is thought to induce shrinkage defects of several hundred micro-sized as shown in Fig. 5(e).

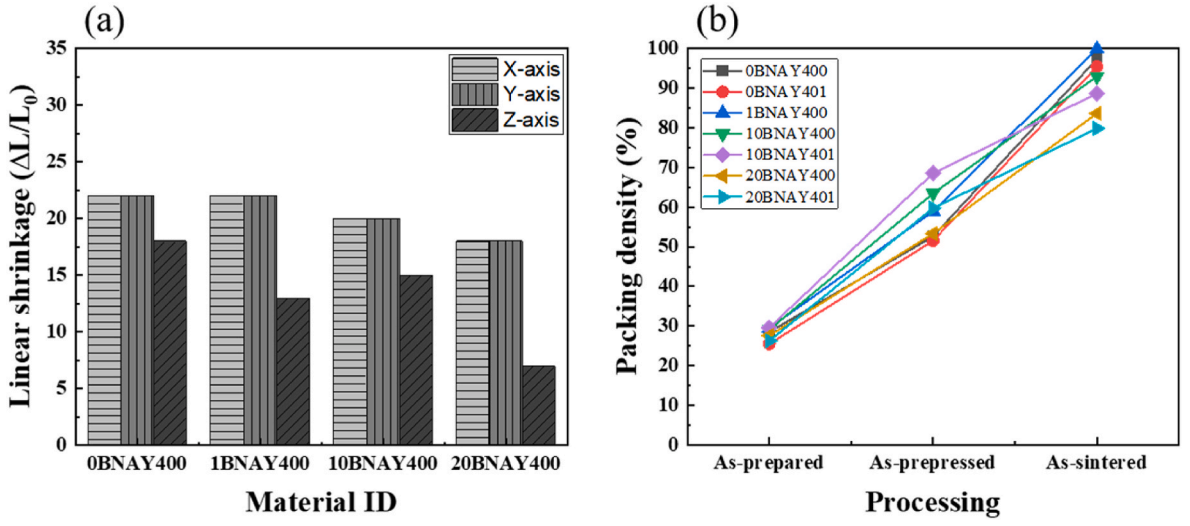


**Fig. 7.** Effects of BN additions on densification behavior of PLPS-SiC fabricated by optimized conditions; (a) linear shrinkage in all directions and (b) packing density in each process.

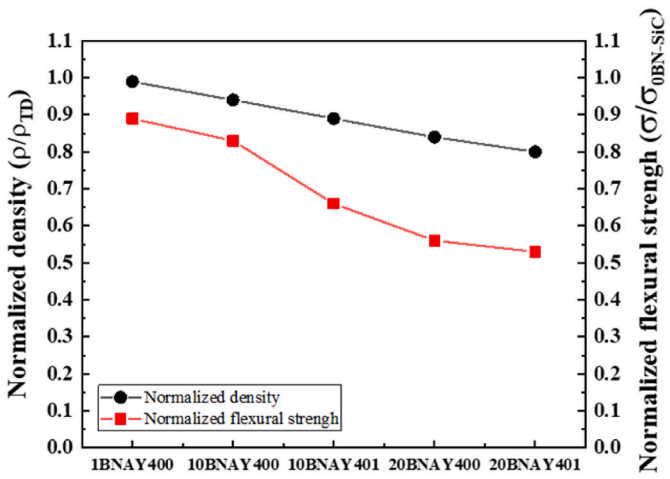


**Fig. 8.** Normalized relative density and flexural strength of BN dispersed PLPS-SiCs fabricated by optimized manufacturing conditions.

### 3.3. Effects of processing parameters on density and mechanical strength

The density and mechanical properties of PLPS-SiCs fabricated using both sintering additives systems were evaluated. Fig. 6(a) shows the normalized density and flexural strength of PLPS-SiC fabricated using only $Al_2O_3$ additive. The relative density and flexural strength of PLPS-SiCs were normalized by the relative density and flexural strength of LPS-SiC fabricated with each sintering additive system. PLPS-SiCs without pressure (A400, A200) appear the relative density corresponding to 95% of LPS-SiC with high pressure during the sintering, as shown in Fig. 6(a). The low pressure of 0.63 MPa during sintering hindered the isotropic densification of PLPS-SiCs (A401, A201), and the densities were similar to that of PLPS-SiC without any pressure applied to the material (A00). The flexural strength of PLPS-SiCs showed a similar tendency to the normalized density of PLPS-SiCs according to the processing parameters. PLPS-SiCs without pressure (A400, A200) showed the flexural strength close to that of the conventional LPS-SiC. The non-isotropic densification by a low external pressure led to relatively many pores inside the material, which is thought to decrease the mechanical strength of the PLPS-SiC. This can also be confirmed in the microstructure images of the PLPS-SiC, as shown in Fig. 4. Fig. 6(b) gives normalized density and flexural strength value of PLPS-SiC fabricated using $Al_2O_3$–$Y_2O_3$ additives. The density was similar to that of the conventional LPS-SiC under three conditions of manufacturing parameters (AY200, AY400, and AY401). However, in terms of strength, only two materials (AY200, and AY400) can achieve the strength close to that of conventional LPS-SiC. The density of AY400 measured using the gas pycnometer was 3.20 g/cm$^3$, which corresponds to 97.3% of the theoretical density, and the open porosity among the total porosity of 2.7% was 0.91%, confirming a fairly low level of open porosity. In the case of AY401. It possesses a density of 3.14 g/cm$^3$, which corresponds to 95.4% of the theoretical density. However, among the total porosity of 4.6%, the open porosity was 2.30%, which was about 2.5 times the open porosity of the AY400. This difference in open porosity led to a decrease in mechanical strength of AY401.

### 3.4. Effects of BN additions on densification behavior, density, and mechanical strength

The densification behavior (linear shrinkage and packing density), density, and mechanical strength of PLPS-SiC with BN particles were also evaluated. The BN addition interfered with the shrinkage of PLPS-SiC. Fig. 7 shows the effects of BN additions on the densification behavior of PLPS-SiC. When 1 vol% of BN was dispersed, the linear shrinkage in the x- and y-axes did not change significantly. However, when the BN amount was increased to 10 vol% and 20 vol%, the linear shrinkage in the x- and y-axes gradually decreased due to the BN additions, as shown in Fig. 7 (a). The linear shrinkages in x- and y-axes decreased with the increase in BN additions. This resulted in low densification, which caused the decrease in bulk density of sintered SiC, as shown in Fig. 7(b). Furthermore, the use of low sintering pressure also caused low densification of BN particle dispersed SiC ceramics. In Fig. 7 (b), the measured packing density after sintering (bulk density) of 20 vol % BN addition materials (20BNAY400 and 20BNAY401) showed the lowest packing densities, 10 vol% BN addition materials (10BNAY400 and 10BNAY401) followed. In the PLPS process without external high pressure applied, heterogeneous BN particles with different sizes and components inside SiC ceramics interfere with bonding by the molten sintering additives, resulting in a decreased bulk density. Fig. 8 shows the normalized density and flexural strength of BN dispersed PLPS-SiC. The density of BN particle dispersion SiC was normalized by the theoretical density of each material, and the strength of BN particle dispersion SiC was normalized by the strength of PLPS-SiC without BN particle fabricated under the same sintering conditions. The following two results could be found by the normalized density by the theoretical density of each material. First, the normalized density (densification) of the sintered material decreased as the amount of BN added increased. Second, when the same amount of BN particles was added, the use of low sintering pressure resulted in a lower density than the materials without low pressure during sintering. In terms of mechanical strength, 20 vol% BN particles dispersed PLPS-SiC exhibited the flexural strength equivalent to the half level of PLPS-SiC without BN addition fabricated under the same conditions. Only materials of 1 and 10 vol% BN particles dispersion, which were not applied to low sintering pressure, showed flexural strength equivalent to above 95% of PLPS-SiC fabricated under the same conditions. The high amount of BN additions and low sintering pressure cause low densification during pressureless sintering, which leads to deterioration in mechanical properties of PLPS-SiC. These findings provide key information for matrix densification and high functionalization in the manufacture of the composite material using PLPS method. Therefore, when manufacturing SiC ceramic and SiC-based CMCs using pressureless sintering, it is necessary to design and modeling suitable for the material applications.

## 4. Discussion

The understanding of the densification behavior for monolithic SiC fabricated by the PLPS method is essential to fabricate $SiC_f$/SiC-matrix composites with a non-pressing process during sintering at high temperatures. In the case of general pressure-assisted sintering using a high sintering pressure, the pressure applied to the powder compact increases the contact points between the SiC particles and the sintering additives, and the final densification of SiC ceramic is easily achieved by the increase in capillary force due to the reduced spacing between the particles. Hence, one way to increase the densification of SiC ceramic without the high sintering pressure is to utilize the capillary force of the molten sintering additives to control the linear shrinkage of the material. Verification in this study indicates that a sufficient amount of the sintering additives molten at sintering temperature can achieve full densification of SiC ceramic by utilizing isotropic shrinkage due to capillary force of liquid phase even when no pressure was used.

Mixture powders without prepressure showed isotropic shrinkage in all directions after sintering. Mixture powders with prepressure showed isotropic shrinkage in x- and y-directions after sintering (Fig. 2). The shrinkage caused by the liquid phase generated during sintering becomes the driving force to form the final sintered body with dense structure from the prepressed powder body with a packing density of about 50% in Fig. 3. As a result, it was shown that the microstructure, density, and strength of PLPS-SiC under some conditions were consistent with that of LPS-SiC sintered with high pressure (Figs. 4–6).

The densities of the BN particle dispersion SiC ceramic were

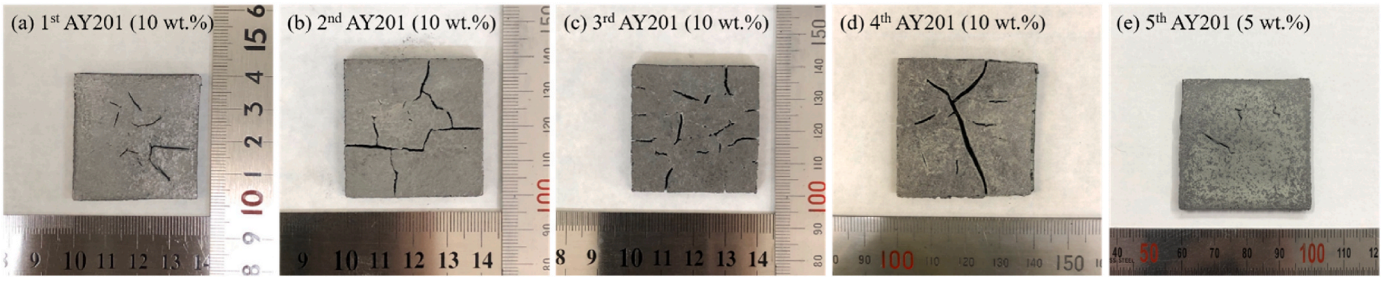


**Fig. 9.** Photos of AY201 ceramic after sintering: 1st trial with 10 wt% of sintering additives, (b) 2nd trial, (c) 3rd trial, (d) 4th trial, and (e) 5th trial with 5 wt% of sintering additives.

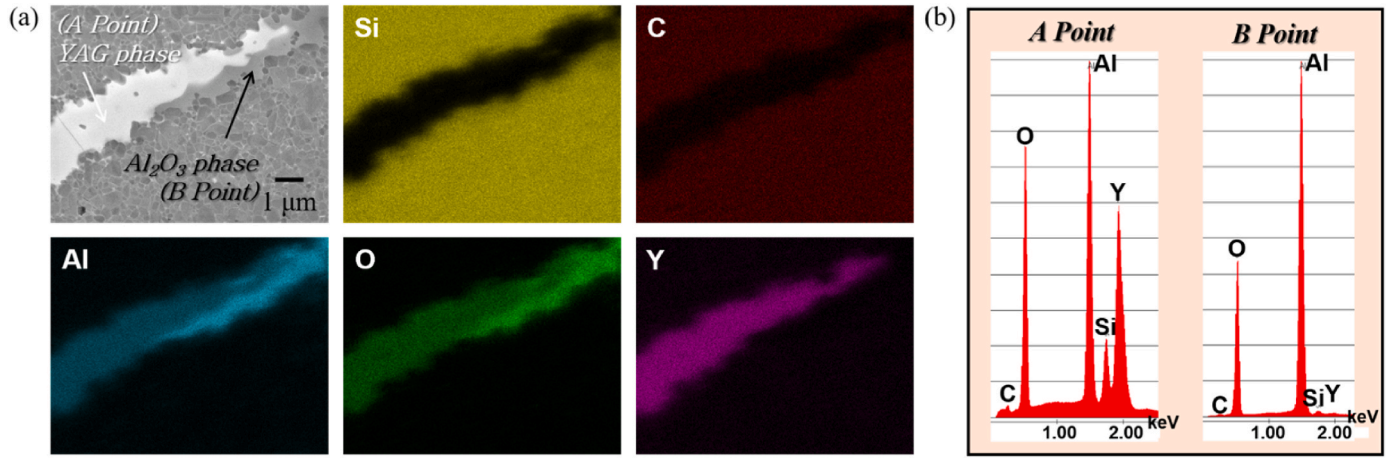


**Fig. 10.** SEM-EDS analysis of agglomerated part of sintering additives in PLPS-SiC, fabricated using $Al_2O_3$–$Y_2O_3$ sintering additives, without pressure; (a) EDS elemental maps, (b) point analysis of A and B potint

normalized to the theoretical density of each material (Fig. 8). PLPS-SiCs with low-pressure showed lower normalized densities than PLPS-SiCs without pressure under the same BN addition amounts. Moreover, PLPS-SiCs dispersed with BN particles of 10 and 20 vol fraction showed significantly different strength trends. In the case of the PLPS-SiC dispersed with 10 vol% BN particles, the material without sintering pressure showed a strength level of about 20% higher than that of the material with low sintering pressure, but the PLPS-SiCs dispersed with 20 vol% BN particles were different. Although no pressure was used during sintering, the PLPS-SiC with 20 vol% BN particles showed a similar level of flexural strength as the material with low sintering pressure. This indicated that there is a critical volume fraction for the BN additions, and this result is expected to greatly affect the PLPS process of the BN particle dispersion $SiC_f$/SiC-matrix composites.

In addition, there are different results according to the sintering additive systems. In the case of only $Al_2O_3$ additive, all PLPS-SiC with low pressure showed low density and reduced densification compared with PLPS-SiCs without pressure. However, in the case of $Al_2O_3$–$Y_2O_3$ additives, AY401 material, which low pressure with 0.63 MPa was applied during sintering also showed a high level of density (densification), as shown in Fig. 6. Furthermore, there are many visible defects in the AY201 material as shown in Fig. 9. Even after several times under the same conditions of a prepressure of 20 MPa, a sintering pressure of 0.63 MPa, and the sintering additives of 10 wt%, the visible defects still existed, and it was confirmed that these visible defects were significantly reduced when the sintering additives were reduced to 5 wt% (Fig. 9(e)). Theoretically, the external pressure applied in the z-direction during sintering causes preferential contact in the z-direction of the powder body. After that, densification occurs by the molten sintering additive to fill the residual pores, but in order to achieve full densification to the x- and y-directions in a sintering region limited by an external force, a sufficient amount of capillary force by the liquid is required. In the case of $Al_2O_3$ additive using the reaction with $SiO_2$ film on the surface of the SiC powder, it is difficult to densify the residual pores in the x- and y-directions due to the local reactions at the surface of the SiC powders, but $Al_2O_3$–$Y_2O_3$ additives using a sufficient amount of liquid phase make this possible. Therefore, they exhibited different microstructures depending on the kind of sintering additives (Figs. 4 and 5). However, it was confirmed that there are agglomeration phenomena of the $Al_2O_3$–$Y_2O_3$ additives as shown in Fig. 10. When a relatively low prepressure with 20 MPa is applied in the powder compact with 10 wt% $Al_2O_3$–$Y_2O_3$ additives, it is considered that a moderate amount (5 wt%) of sintering additive is required rather than a sufficient amount (10 wt%). This result also means that it is necessary to optimize the PLPS-SiC ceramics according to the sintering process (pre- and sintering pressure). In general pressure-assisted LPS process, prepared mixture powders are heated to a temperature where liquid forms in the initial stage of sintering. When liquid forms inside powder compacts, grain rearrangement and solution-reprecipitation stages for densification occur. During grain rearrangement and solution-reprecipitation stages, external force by hot-pressing was applied to powder compact. The assisted external force during the densification steps can help the contact between the SiC particles, and the particles at closer distances enter the final densification stage through a solution-reprecipitation stage which proceeds by mass transport such as surface and grain boundary diffusion by the liquid phase [25,26]. It seems that the external pressure of 20 MPa can prevent the agglomeration phenomena of sintering additives due to the constrained environment of the powder compact. Without assisted high pressure, we were able to confirm the agglomeration phenomenon of sintering additives, as shown in Fig. 10 (a). According to SEM-EDS (energy-dispersive x-ray spectroscopy) analysis, the agglomerated parts of sintering additives were identified as yttrium aluminum garnet (YAG)

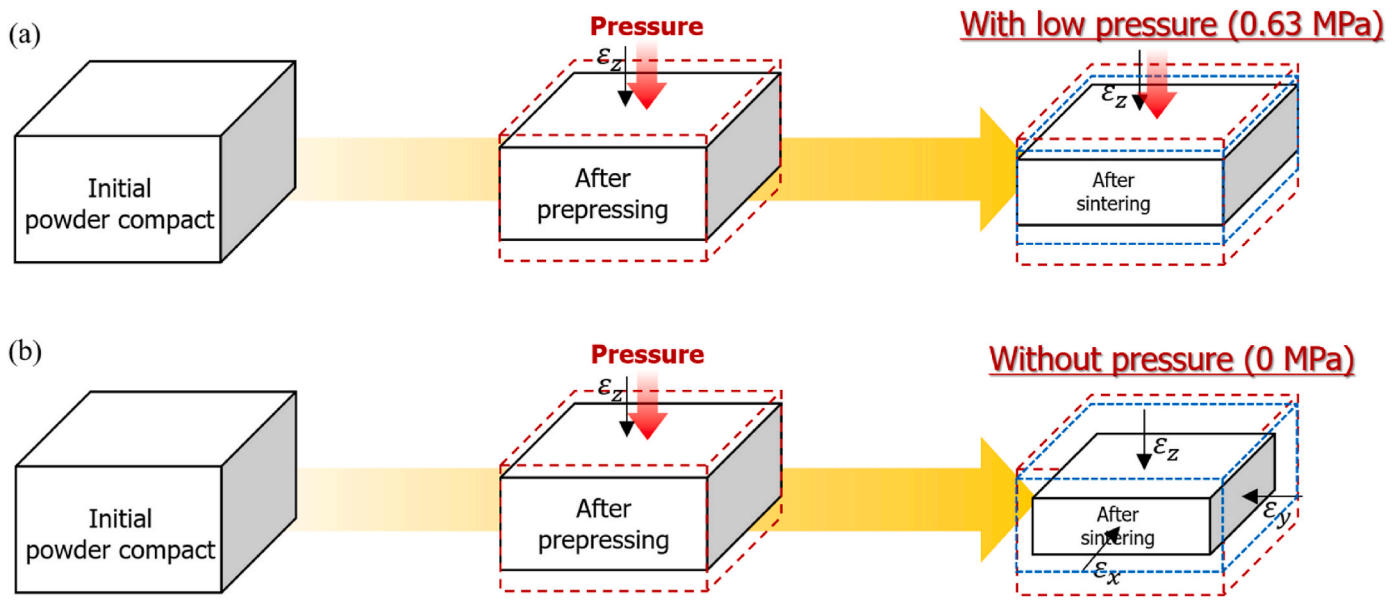


**Fig. 11.** The schematic diagram of densification behavior for pressureless liquid phase sintering (a) with and (b) without low pressure.

and $Al_2O_3$ phases (Fig. 10(b)). Aluminum, yttrium, and oxygen elements, which were in the agglomeration of sintering additives, were clearly detected in PLPS-SiC without pressure fabricated using $Al_2O_3$–$Y_2O_3$ additives. The capillary force of the sintering additive molten at the temperature above the eutectic point attracts SiC particles and causes densification by isotropic shrinkage but also causes agglomeration phenomenon due to the attraction force between the molten sintering additives. However, this agglomeration phenomenon could be confirmed only when $Al_2O_3$–$Y_2O_3$ mixtures were used as the sintering additives, and in the case of only $Al_2O_3$ additive utilizing thin $SiO_2$ film on the surface of SiC powder, the agglomeration phenomenon was not confirmed.

As mentioned in the results and discussion section, the heterogeneity in matrix components affected the densification of PLPS-SiC ceramic, which was the reason for the degradation in the density and strength of the material. However, under some conditions in which a small amount (10 vol%) of BN was added, the strength equivalent to about 85% of the PLPS-SiC without BN and a density of about 95% were exhibited. In order to apply the PLPS method to the BN particle dispersion $SiC_f$/SiC-matrix composites, which have no interface material developed in our laboratory, the investigation of SiC fiber and BN particle could be the next step.

## 5. Conclusions

As a preliminary investigation for matrix consolidation of $SiC_f$/SiC composites, the process parameters for monolithic SiC have been successfully optimized via PLPS method using the capillary force of the molten sintering additives at the temperature above the eutectic point. PLPS-SiCs were processed in a simple two-step procedure that included prepressing the powder green compact followed by pressureless liquid-phase sintering of SiC nano-powder and sintering additives. PLPS-SiCs using $Al_2O_3$–$Y_2O_3$ mixtures and/or only $Al_2O_3$ as the sintering additives can achieve full densification, and possess high mechanical strength close to that of conventional LPS-SiC. However, the optimized parameters were slightly different depending on the types of sintering additive. PLPS-SiC using $Al_2O_3$–$Y_2O_3$ mixtures as the sintering additives, was prepared through a prepressure with 20 MPa and no sintering pressure, exhibited the highest bulk density of 3.29 g/cm$^3$ and flexural strength of 501 ± 10 MPa. In the case of PLPS-SiC using only $Al_2O_3$ as the sintering additive, PLPS-SiC prepared through a prepressure with 40 MPa and no sintering pressure showed the highest bulk density of 3.08 g/cm$^3$ and flexural strength of 471 ± 61 MPa. The densification behavior for fabricated PLPS-SiC using both kinds of sintering additives was demonstrated by the isotropic shrinkage via the capillary force of the molten sintering additives, as shown in Fig. 11(b). When a low pressure of 0.63 MPa is used during the sintering (Fig. 11(a)), the isotropic densification by the capillary force of the molten sintering additives is interfered with by an external constrained force in z-axis, resulting in only z-direction shrinkage. Densification of BN particle dispersed PLPS-SiC became difficult with increasing BN particle additions. Increasing the BN particle additions leads to heterogeneity of matrix components in PLPS-SiC, which hinders the isotropic shrinkage of the PLPS-SiC, and thereby increase the porosity and decreases the mechanical strength. The critical volume fraction for the BN addition amount was also identified. To obtain a SiC ceramics with the dense microstructure by the pressureless liquid phase sintering method, it is necessary to control the isotropic shrinkage via the capillary force of molten sintering additives.

## Declaration of competing interest

The authors declare that they have no known competing financial interests or personal relationships that could have appeared to influence the work reported in this paper.

## Acknowledgement

This research was funded by Japan Science and Technology Agency (JST) Grant Number:JPMJOP1841.

## References

[1] W.R. Corwin, T.D. Burchell, Y. Katoh, T.E. Mcgreevy, R.K. Nanstad, W. Ren, L. L. Snead, D.F. Wilson, Generation IV Reactors Integrated Materials Technology Program Plan: Focus on Very High Temperature Reactor Materials, Technical Report, Oak Ridge National Lab., 2008, p. 129.
[2] M.A. Futterer, L. Fu, C. Sink, S. de Groot, M. Pouchon, Y.W. Kim, F. Carre, Y. Tachibana, Status of the very high temperature reactor system, Prog. Nucl. Energy 77 (2014) 266–281.
[3] Y. Katoh, K. Ozawa, C. Shih, T. Nozawa, R.J. Shinavski, A. Hasegawa, L.L. Snead, Continuous SiC fiber, CVI SiC matrix composites for nuclear applications: properties and irradiation effects, J. Nucl. Mater. 448 (2014) 448–476.
[4] T. Nozawa, K. Ozawa, C.H. Park, J.S. Park, A. Kohyama, A. Hasegawa, S. Nogami, T. Hinoki, S. Kondo, T. Yano, T. Shibayama, B. Tsuchiya, T. Shikama, S. Nagata,

T. Tanaka, H. Iwakiri, Y. Yamamoto, S. Konishi, R. Kasada, M. Kondo, T. Kunugi, T. Yokomine, Y. Ueki, N. Okubo, T. Taguchi, H. Tanigawa, Japanese activities of the R&D on silicon carbide composites in the broader approach period and beyond, J. Nucl. Mater. 511 (2018) 582–590.

[5] T. Nakamura, T. Oka, K. Imanari, K. Shinohara, M. Ishizaki, Development of CMC turbine parts for aero engines, IHI, Technical Articles 47 (2014) 29–32.

[6] T. Kameda, Y. Itoh, T. Hishata, T. Okamura, Development of Continuous Fiber Reinforced Reaction Sintered Silicon Carbide Matrix Composite for Gas Turbine Hot Parts Application, ASME, 2000, 2000-GT-67.

[7] C.M. Grondahl, T. Tsuchiya, Performance benefit assessment of ceramic components in an MS9001FA gas turbine, J. Eng. Gas Turbines Power 123 (2001) 513–519.

[8] Y. Katoh, K. Ozawa, C. Shih, T. Nozawa, R.J. Shinavski, A. Hasegawa, L.L. Snead, Continuous SiC fiber, CVI SiC matrix composites for nuclear applications: properties and irradiation effects, J. Nucl. Mater. 448 (2014) 448–476.

[9] S.P. Lee, Y. Katoh, J.S. Park, S. Dong, A. Kohyama, S. Suyama, H.K. Yoon, Microstructural and mechanical characteristics of SiC/SiC composites with modified-RS process, J. Nucl. Mater. 289 (2001) 30–36.

[10] M. Kotani, T. Inoue, A. Kohyama, K. Okamura, Y. Katoh, Consolidation of polymer-derived SiC matrix composites: processing and microstructure, Compos. Sci. Technol. 62 (2002) 2179–2188.

[11] S. Dong, Y. Katoh, A. Kohyama, Processing optimization and mechanical evaluation of hot pressed 2D Tyranno-SA/SiC composites, J. Eur. Ceram. Soc. 23 (2003) 1223–1231.

[12] K. Shimoda, J.S. Park, T. Hinoki, A. Kohyama, Influence of pyrolytic carbon interface thickness on microstructure and mechanical properties of SiC/SiC composites by NITE process, Compos. Sci. Technol. 68 (2008) 98–105.

[13] G.N. Morsher, J.D. Cawley, Intermediate temperature strength degradation in SiC/SiC composites, J. Eur. Ceram. Soc. 22 (2002) 2777–2787.

[14] S. Ochiai, S. Kimura, H. Tanaka, M. Tanaka, M. Hojo, K. Morishita, H. Okuda, H. Nakayama, M. Tamura, K. Shibata, M. Sato, Degradation of SiC/SiC composite due to exposure at high temperatures in vacuum in comparison with that in air, Compos. Part A Appl. Sci. Manuf. 35 (2004) 33–40.

[15] R. Naslain, A. Guette, F. Rebillat, S. Le Gallet, F. Lamouroux, L. Filipuzzi, C. Louchet, Oxidation mechanisms and kinetics of SiC-matrix composites and their constituents, J. Mater. Sci. 39 (2004) 7303–7316.

[16] T. Hinoki, T. Kanayama, S. Ogitani, S. Fukuhara, K. Kamoshida, K. Shimoda, N. Tsurui, S. Hokari, Development of oxidation resistant BN particle dispersion SiC composites, Bullet. Ceramic Soc. Jpn (2020) 423–426.

[17] M. Khodaei, O. Yaghobizade, S.H.N. Alhosseini, S. Esmaeeli, S.R. Mousavi, The effect of oxide, carbide, nitride and boride additives on properties of pressureless sintered SiC: a review, J. Eur. Ceram. Soc. 39 (2019) 2215–2231.

[18] H. Liang, X. Yao, H. Zhang, X. Liu, Z. Huang, In situ toughening of pressureless liquid phase sintered α-SiC by using $TiO_2$, Ceram. Int. 40 (2014) 10699–10704.

[19] K.J. Kim, J.H. Eom, Y.W. Kim, W.S. Seo, M.J. Lee, S.S. Hwang, Highly resistive SiC ceramics sintered with $Al_2O_3$-AlN-$Y_2O_3$ additions, Ceram. Int. 43 (2017) 5343–5346.

[20] J.Y. Lee, S.P. Lee, J.K. Lee, M.H. Lee, S.K. Hwang, Mechanical properties of liquid phase sintered SiC materials by the addition of unimodal and bimodal particles, Korean J. Met. Mater. 57 (2019) 60–66.

[21] S.P. Lee, M.H. Lee, J.K. Lee, A. Kohyama, J.H. Lee, High temperature characterization of LPS-SiC based materials with oxide additives, J. Nucl. Mater. 386–388 (2009) 483–486.

[22] K. Shimoda, T. Hinoki, A. Kohyama, Effect of additive content on transient liquid phase sintering in SiC nanopowder infiltrated $SiC_f$/SiC composites, Compos. Sci. Technol. 71 (2011) 609–615.

[23] K. Shimoda, A. Kohyama, T. Hinoki, High mechanical performance SiC/SiC composites by NITE process with tailoring of appropriate fabrication temperature to fiber volume fraction, Compos. Sci. Technol. 69 (2009) 1623–1628.

[24] A. Noviyanto, The effect of polysilazane on the densification and mechanical properties of $SiC_f$/SiC composites, SINERGI 24 (2020) 11–16.

[25] R.M. German, Sintering Theory and Practice, John Wiley & Sons, INC., 1996, pp. 225–312.

[26] J. Rojek, S. Nosewicz, M. Mazdziarz, P. Kowalczyk, K. Wawrzyk, D. Lumelskyj, Modeling of a sintering process at various scales, Procedia Eng. 177 (2017) 263–270.